# Progress at the Vatican Advanced Technology Telescope

West, Steve, Nagel, Robert, Harvey, David, Brar, A., Phillips, B., et al.

Steve C. West, Robert H. Nagel, David Allen Harvey, A. Brar, B. Phillips, J. Ray, Thomas J. Trebisky, Richard H. Cromwell, Neville J. Woolf, Chris Corbally, R. Boyle, Daniel R. Blanco, L. Otten, "Progress at the Vatican Advanced Technology Telescope," Proc. SPIE 2871, Optical Telescopes of Today and Tomorrow, (21 March 1997); doi: 10.1117/12.268968

Event: Optical Telescopes of Today and Tomorrow, 1996, Landskrona/Hven, Sweden

# Progress at the Vatican Advanced Technology Telescope

S. C. West, R. H. Nagel, D. Harvey, A. Brar, B. Phillips, J. Ray, T. J. Trebisky, R. Cromwell, and N. J. Woolf (Steward Observatory)
C. Corbally and R. Boyle (Vatican Observatory Research Group)
D. Blanco (National Optical Astronomy Observatories)
L. Otten (U. Seattle)

## 1.0 Abstract

The Vatican Advanced Technology Telescope incorporates a fast (f/1.0) borosilicate honeycomb primary mirror and an f/0.9 secondary in an aplanatic Gregorian optical configuration. We provide a brief technical and performance overview by describing the optical layout, the primary and secondary mirror systems, and the telescope drive and control system. Results from a high resolution wavefront sensor and a current wide-field image taken at the f/9 focus demonstrates the overall fine performance of the telescope.

KEYWORDS: telescopes, mirror supports, thermal control, wide-field imaging, wavefront sensing, servos.

## 2.0 Facility

The Vatican Advanced Technology Telescope (VATT) is a cooperative effort between the University of Arizona Steward Observatory (UA) and the Vatican Observatory Research Group (VORG). Located atop Mt. Graham at 3.2-km (10,500-ft) altitude, it serves as a demonstration of technology planned for larger telescope projects by the UA and other collaborators. A photograph of the facility taken in December 1994 is shown in Figure 1.

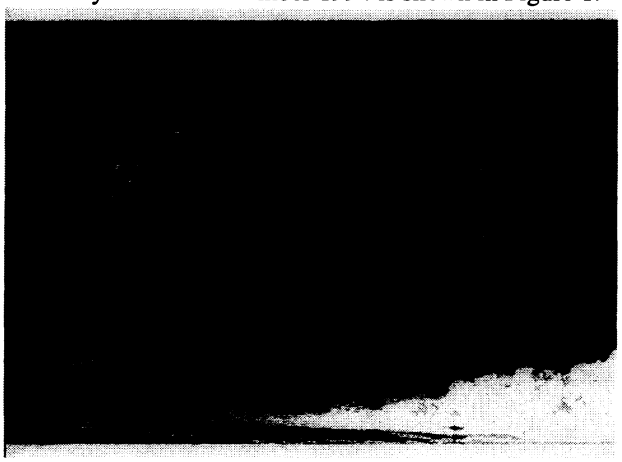

**FIGURE 1. Located at the Mt. Graham International Observatories site in southeastern Arizona, the VATT was completed in 1995.**

The VATT's construction and subsequent operation were funded by generous contributors to the Vatican Observatory Foundation, a U.S. incorporated tax-exempt foundation. Its two components, the Alice P. Lennon Telescope and the Thomas J. Bannan Astrophysics Facility, were named after principal benefactors. The University of Arizona Steward Observatory contributed the primary mirror which is one quarter of the project's cost. M3 Engineering (Tucson, AZ) designed the facility.

## 3.0 Telescope Optics

The Vatican Advanced Technology Telescope (VATT) is an aplanatic Gregorian (AG). The optical prescription is shown in Figure 2. Both the primary and secondary mirrors are ellipsoidal. The maximum field of view (15 arcminutes diameter) is limited by field curvature and astigmatism. The Gregorian configuration was chosen mainly because a concave



0277-786X/97/$10.00

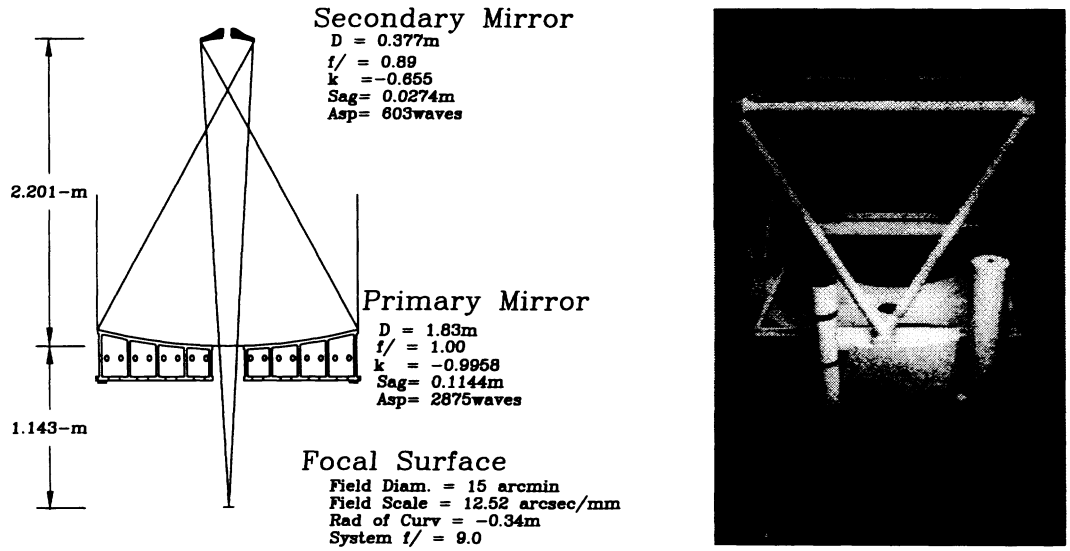


**FIGURE 2. Optical prescription of the aplanatic Gregorian VATT and a picture of the installed mount.**

secondary mirror was considerably less expensive to test than a convex mirror. The 560-kg 1.83-m diameter honeycomb borosilicate primary mirror was manufactured at the Steward Observatory Mirror Laboratory. It was spun cast to achieve f/1.0 curvature of the faceplate and was the first mirror to be polished using the stressed-lap technique.[1-4]

The VATT secondary mirror is an f/0.9 ellipsoid on a 0.38-m diameter single-arch Zerodur substrate that weighs 30.6-kg. It is has a simple central support via a flanged central hole.[5,6] The mirror was generated and polished by the Space Optics Research Lab (Chelmsford, MA).[7]

The final interferogram for each mirror is shown in Figure 3.

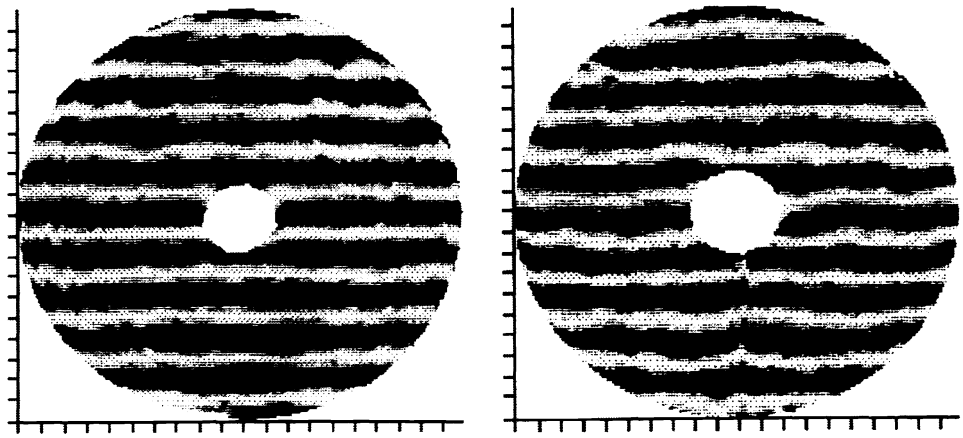

**FIGURE 3. Synthetic interferograms of the finished primary (left) and secondary mirrors (obtained from averages of 15 phase maps). The 1.8-m f/1.0 ellipsoidal primary mirror was stressed-lap polished at Steward Observatory to a surface error of 17-nm rms and 170-nm p-v. The Strehl ratio is 90% at 633-nm. The phase maps were obtained with a Shack cube interferometer and refractive null corrector. The 0.38-m f/0.9 concave ellipsoidal secondary mirror was polished at Space Optics Research Labs. The final figure was measured at the Steward Observatory to be 13-nm rms and 150-nm p-v surface error with a Strehl ratio of 98.5% at 633-nm. The phase maps of the secondary mirror were obtained with a double-pass interferometer having a Shack cube at one focus of the ellipse and a precision ball bearing reflector at the other focus (the vertical feature is the rod holding the bearing).**

# 4.0 Primary Mirror Cell

## 4.1 Supports

The relatively stiff 1.83-m diameter mirror has relaxed support requirements compared to larger mirrors. The primary mirror cell is shown in Figure 4. The positions of the 36 pneumatic axial actuators and 16 elevation-oriented passively

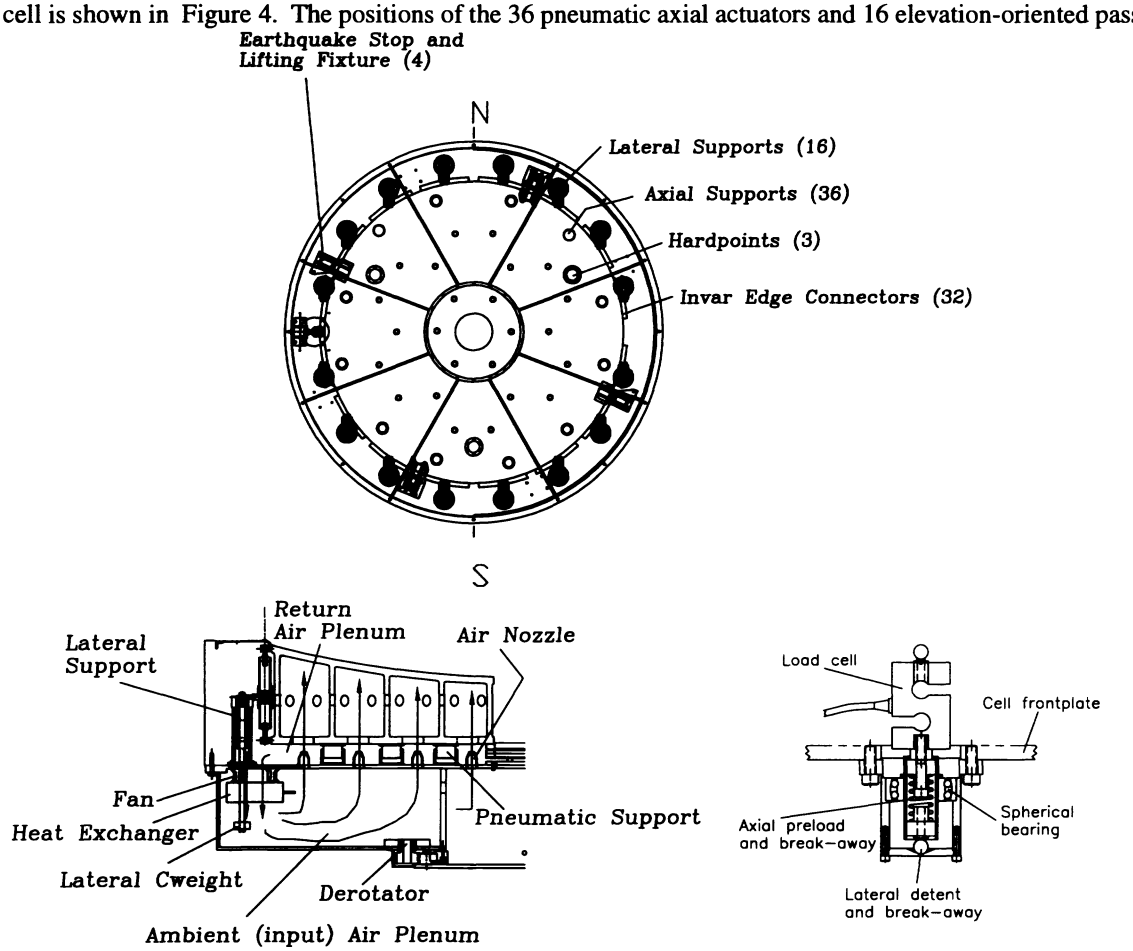


**FIGURE 4. Top and side views of the VATT primary mirror cell showing schematics of the mirror supports, earthquake stops, lifting fixtures, and thermal control system. One of the 3 hardpoints is detailed in the lower right. It combines a force-sensor feedback for the pneumatic support servo with lateral and axial positioning reference and high-force break aways.**

counterweighted lateral actuators were determined from finite element models.[8,9] The axial actuators are placed at the honeycomb rib intersections and the lateral actuators are attached to invar bars glued to the edges of the mirror front and back plates. The inner 12 actuators have peak forces of 112.2-N, the middle 12 actuators have 120.7-N peak forces, and the outer 12 have 225.1-N. The corresponding mirror surface deformation determined from the finite-element models is 5.4-nm rms (30-nm p-p) at zenith and 5.8-nm rms (40-nm p-p) at horizon pointing. The actual implementation however contains 2 unique axial force actuators (inner 24 vs. outer 12) with area ratios of 2 connected to a common pressure head that is further divided into 3 radial sectors in order to control mirror tilt. Each sector contains a stiff hardpoint that provides a positioning reference that incorporates both axial and lateral high-force break-aways and an axial force measuring load cell for servo control of the pressure head.

## 4.2 Thermal Control

The main functions of the primary mirror thermal control are to eliminate figure distortion by maintaining temperature uniformity of the mirror and to force the mirror to track ambient temperature to avoid local seeing effects. These requirements are achieved through forced air convection of the inside of the honeycomb structures.[10,11] The specifications for the thermal control system are:[12]

- Maintain isothermality of mirror blank to $0.1°C$ (keep gradients small to avoid figure distortion).
- Hold faceplate within $\pm 0.1°C$ of ambient (reduce effects of local seeing).
- Achieve glass temperature slew rates of up to $2°C$/hr.
- Deliver adequate forced air to achieve a glass temperature time constant of 30-minutes (avoids having to predict ambient temperature *a-priori*).
- Exert < 40-Pa pressure variation to the mirror (avoids figure distortion due to uneven plenum pressure distribution).
- Air delivery must not induce more than 20-nm lateral vibration amplitude at any frequency (controls wavefront tilt).

Figure 4 also illustrates the air flow for a single VATT ventilator unit. A fan (Patriot PD48B2) pulls air out of the return plenum and pressurizes the input plenum. A heat exchanger (Lytron 6210-G1) isothermalizes the air and brings it to ambient temperature. The air is then forced into the honeycomb cells through backplate perforations via 82 air nozzles at an air pressure of ~30-Pa across each nozzle. Eight ventilators are evenly distributed about the cell perimeter, and provide 7-liters/sec of air volume to each honeycomb cell.

A schematic of the thermal system is shown in Figure 5. The off-board chiller (Neslab HX150) supplies a water-glycol

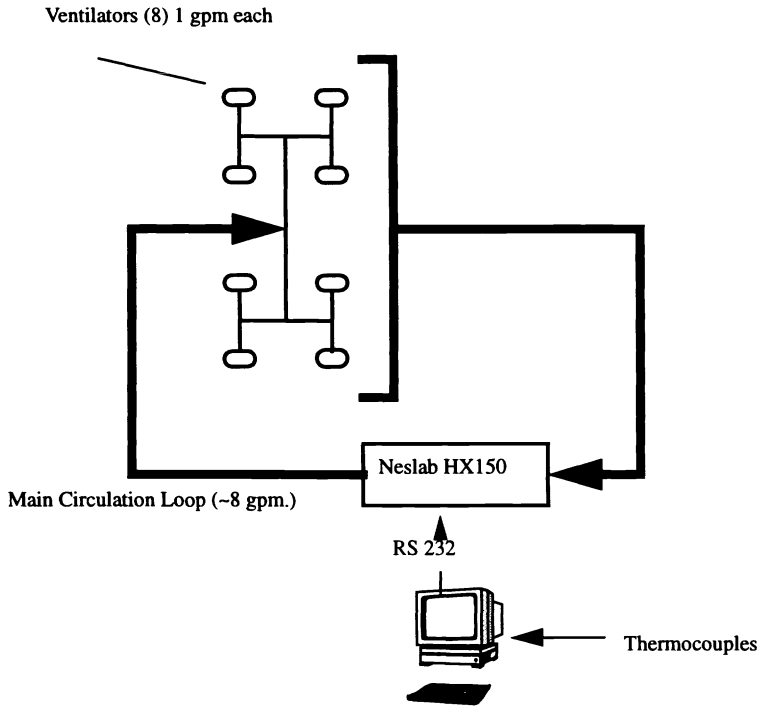


**FIGURE 5. Plumbing and control loop for the primary mirror thermal control system. The air-cooled compressor of the Neslab chiller-recirculator dumps heat into a thermally managed room.**

mixture to the on-board heat exchangers for removal of heat from the cell weldment, mirror, and ventilation fans. It is located in a thermally managed room 12-m below the telescope. The chiller is capable of removing 0.5-kW of heat even at low temperature extremes of $-15°C$ which is adequate to slew the cell and mirror by $1°C$/hr. The on-board

plumbing uses multiple "T" connections to balance the flow rate through the ventilators. A Neslab CP55 pump provides 30-L/min (8-gpm) liquid circulation. The chiller is programmed by a VxWorks computer instrumented with thermocouples reading dome ambient (target) and mirror temperature (feedback).

## 5.0 Secondary Mirror Positioner

The secondary mirror must be precisely positioned relative to the primary mirror. To achieve our goal of 0.1-arcsecond rms images, active collimation is essential because: 1) the predicted gravity deflection of the telescope structure (30-$\mu m$) is larger than the collimation decenter requirement, and 2) a $0.1°C$ temperature change causes the 2-m optical support structure to change length by the entire focus error budget (see section 7.0).

Figure 6 shows the 6-axis positioner for the secondary in the "mirror-up" orientation. The tripod has a hole in the mid-

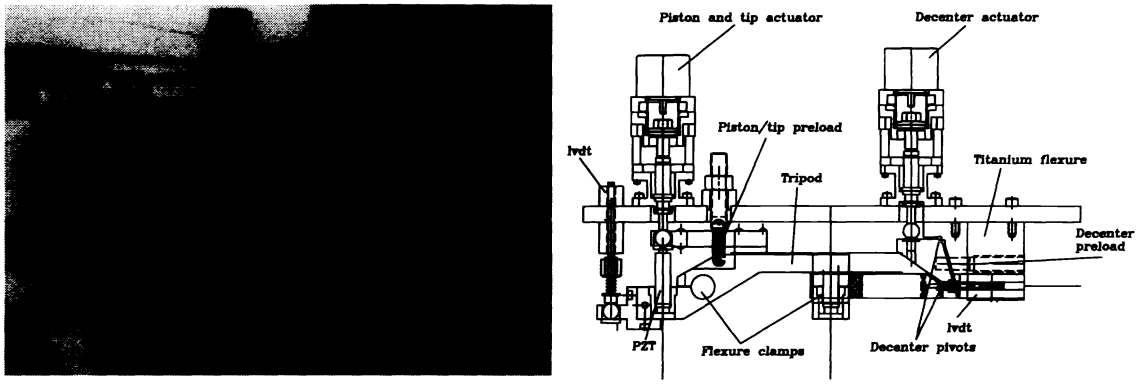


**FIGURE 6. A picture of the six-axis positioner for the VATT secondary (mirror-up). The right drawing shows details of the tip and decenter actuators (mirror-down). Each drive consists of a stepper motor geared through a harmonic drive and fine pitch lead screw that push on a dual-axis titanium flexure. The inline piezo stacks provide for active correction of atmosphere (not yet implemented). The lowest resonant frequency is 30-Hz.**

dle for connection to the central hub support in the mirror. The tripod is positioned with 3 decenter actuators connected perpendicular to each tripod arm and 3 tip-piston actuators connected to the tripod ends. Six lvdts measure lateral and piston displacements. Each drive consists of a stepping motor geared through a harmonic drive and micrometer screw resulting in a decenter resolution of $< 0.1$ $\mu m$/step, a despace resolution of 0.2 $\mu m$/step, and a tip-tilt resolution of 0.2 arcsecond/step.

The details of the actuators are also shown in Figure 6. Each arm of the tripod has both a decenter and tip actuator. The figure shows the decenter actuator for the tripod arm sticking out of the page and the tip-piston actuator for the tripod arm to the left. The tripod is pulled up against the three tip actuators by three tension spring preloads. The tip and piston of the mirror is controlled by the extension of the micrometer screw actuator. A PZT is placed in series with the screw to provide high frequency tip-tilt correction of the atmosphere (not yet implemented). Preliminary tests show that the positioner has its lowest tip-tilt resonance near 30-Hz.

The decenter actuator acts through two pivots in a titanium flexure in order to convert axial into lateral motion. The flexure is clamped tangent to a tripod arm. A compression spring preload keeps the flexure loaded against the actuator screw.

Because of the tight collimation requirements, this positioner must be accurately calibrated. A granite box-parallel was attached to the tripod and instrumented with a kinematic set of contact lvdts in order to find the influence of each actuator on the rigid body motion of the tripod. The result is a 6 x 6 matrix that transforms the desired cartesian motion of the secondary mirror into feedback voltage increments for the positioner.

# 6.0 Mount and Telescope Control System

## 6.1 Axes and Control

The optical support structure and alt-azimuth mount were built by L & F Industries and Paragon Engineering (Figure 2) and allow a 1.8-m telescope to fit within a 7-m diameter dome.[13] The 12,000-kg of moving mass is supported on a 12-pad hydrostatic azimuth bearing. Excluding the pier, the lowest resonant frequency is near 19-Hz.

The altitude and azimuth motors are surplused 1.2-m diameter CAT scan direct-drive brushed DC torque motors each capable of producing 1360-Nm of torque (Sierracin Magnedyne). The 80-kHz PWM Copley amplifiers are filtered to be RFI-free. The resulting motion is extremely smooth and free of cogging and periodic errors inherent in gear-driven systems. Both axes use friction-drive incremental encoders (Heidenhain ROD800) to derive both the position and velocity feedback. Combined with 25x interpolators, final resolutions on the sky are ~60-pulses/arcsecond for both axes. The de-rotator uses a precision 1114:1 dynamically-preloaded spur-gear reducer. An incremental encoder provides control loop feedback with 0.11-arcsecond positional resolution. Tracking normally requires 20-Nm of torque and occasionally up to 600-Nm in stiff winds.

Rather than using tachometers, the velocity is obtained digitally in hardware using an LM628-based VME servo card which samples the encoders and updates the command voltages to the DC torque motor amplifiers at a 3-kHz rate. Position-loop control is closed with software in the VxWorks machine updating the 32-bit registers in the LM628 at a 100-Hz rate. A Sony MagneSwitch provides a reference start-up position for each axis. The maximum slew velocity is 8-deg/sec given by the maximum pulse rate of the encoders, but is limited to 2-deg/sec for safety reasons.

## 6.2 Mount Hardware

The VATT telescope control system (TCS) hardware consists of a single VME Bus incorporating a Motorola VME 147 CPU with Ethernet hardware for communications to a SUN Ultra host computer. Axes control uses a 3-channel Green Spring IP-LM628 servo control card which reads the incremental encoders and closes the three velocity loops. A GMS digital I/O board controls and senses various digital signals (mirror cover, dome position and shutter, fans, subsystem power, elevation axis air brake, and counterweight motors). The dome rotation servo system is handled with a Burr Brown MPV 904 DAC VME-board.

Secondary mirror position feedback is acquired with a 16-bit Acromag 9330 ADC from 6 lvdt sensors. This board also provides access to counterweight and servo amplifier currents used to auto-balance the telescope. An Oregon Micro Systems VME8 stepper motor control board is used to drive the secondary mirror actuators.

Serial communications to low bandwidth intelligent telescope subsystems such as the primary mirror thermal control and the offset guider motion control is provided by a 6-port VME Force serial I/O board. A separate serial port communicates with an external GPS clock that provides accurate date and time for system initialization and produces a precision 1-kHz time base for the TCS software.

Guiding and object acquisition capabilities are handled through an Eltec 8-bit VME video frame grabber that digitizes video from the Photometrics ATC-5 CCD camera attached to the offset guider.

## 6.3 Software

The user interface is provided by a Motif-style windowed GUI displayed on a SUN Microsystems Sparc Ultra main console which also acts as a host computer for the control system's real-time OS, control software, and databases via standard TCP/IP ethernet communications.

Since the TCS is run from a single computer system, Wind River's VxWorks multi-tasking/multi-threaded Operating System was chosen because of its compact and robust real time capabilities. In addition Wind River's Wind-X X-Win-

dows driver software is used to generate the GUI on the host SUN computer. A view of the engineering VATT TCS Run-time GUI is shown in Figure 7.

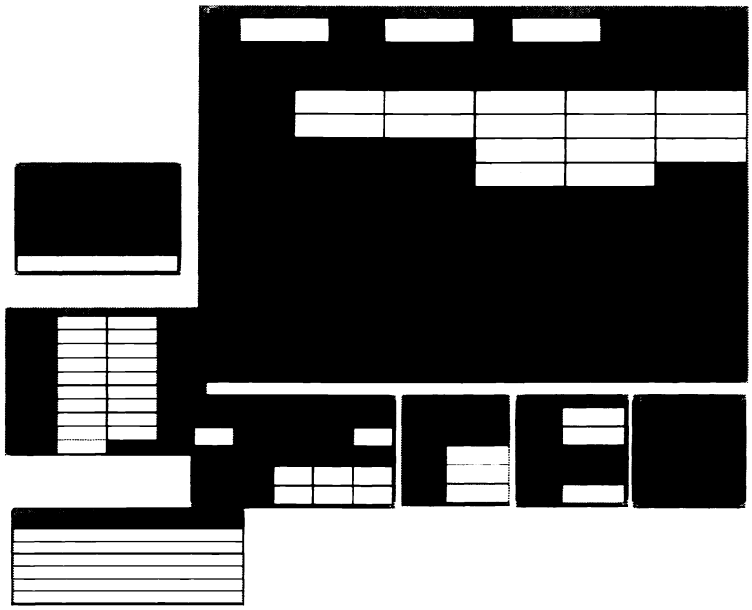

**FIGURE 7. The VATT TCS client software is written in "C" and displayed as a Motif-style GUI. Processing is distributed into 6 main tasks. The Servo task has the highest priority and is triggered by a 1-kHz interrupt from the GPS clock. Other tasks manage the secondary mirror control system, primary mirror thermal and axial support system, paddle/auto-guiding, and object catalog databases.**

### 6.3.1 The Servo Control Task

The Servo Control Task is interrupt driven and is responsible for overall control of the mount and the field de-rotator. Every 1/100th-second the control loop takes the user specified right ascension and declination and adds in any commanded bias rates (*e.g.* tracking comets and asteroids) to construct a new commanded position. This new RA and Dec is transformed into altitude, azimuth and de-rotator angles using the system computed LST. The altitude is then corrected for the effects of atmospheric refraction. The new altitude and azimuth are then corrected for telescope flexure and mount misalignments and converted into commanded positions in encoder counts. These encoder-based positions are then fed to the three axial software Servo position loops diagrammed in Figure 8.

As previously mentioned, an LM628 Servo board functions as a digital tachometer. This board runs a standard PID loop in hardware and takes velocity commands from the Servo Control task. The software position loop is a modified PID algorithm incorporating a square root approach for the Type 0 loop and a detachable integrator loop for the Type 1 and Type 2 loops. Gains, switch points, and limits are user definable to accommodate systems of various bandwidths and resonances.

## 6.4 Performance and Upgrades

Pointing data runs recently performed using the VATT have enabled accurate modeling of telescope flexure and misalignments The analytic modeling software produced by Patrick Wallace of the Rutherford Appleton Laboratory in the UK called Tpoint was used to map the misalignments and inherent flexures of the system. Study of the mount using this software indicates that despite the nearly 0.26-degree zenithal alignment error, the telescope is capable of pointing to better than 4-arcseconds over it's entire range of motion. In addition, tests performed using unguided CCD imaging

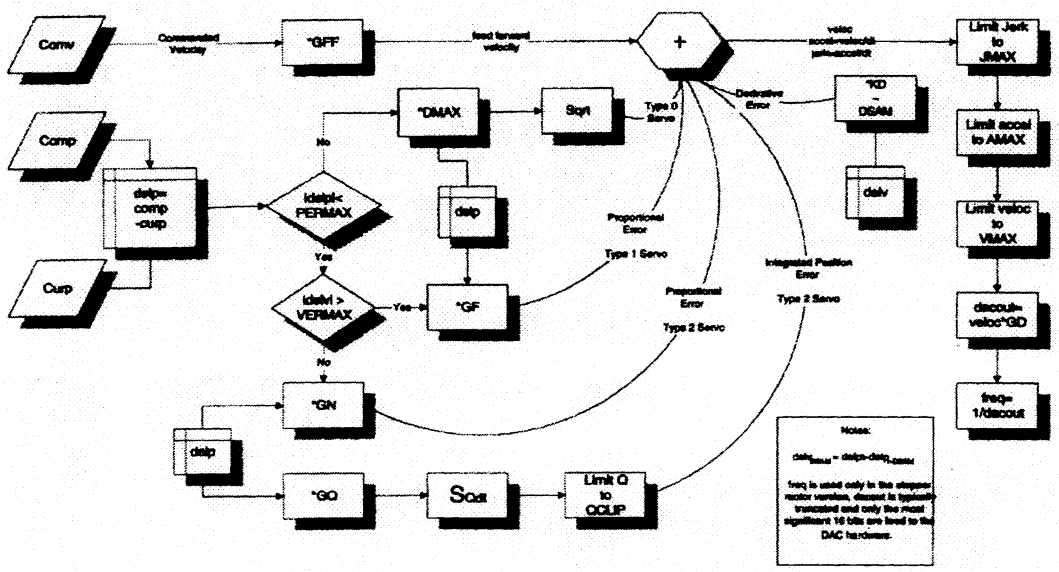


**FIGURE 8. Flowchart of the servo control software PID loop used to provide velocity commands to the digital tachometer.**

confirm tracking accuracy of better than 1-arcsecond over a 7-minute interval. Figure 9 shows the final pointing accu-

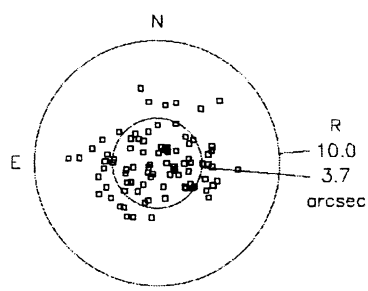


**FIGURE 9. The VATT pointing error scattergram after the removal of mount flexure and misalignment effects. Currently, the VATT is pointing to 3.63-arcseconds rms measured over the entire sky.**

racy after removal of mount misalignment and flexure as modeled by Tpoint.

Currently the VATT TCS is undergoing a major facelift of it's Engineering GUI including the addition of robust autoguiding software which will automatically scan various on-line star catalogs for optimal selection of guide stars, a more compact and "astronomer friendly" (rather than "engineer" handy) Window and menu system better suited to astronomical observing, integrated network access for smart instrumentation and remote observing, and a more equitable distribution of system control tasking using client software running on the SUN host.

## 7.0 Optical Alignment

Exacerbated by the increased sensitivity of coma on secondary misalignment for the Gregorian design compared to an equivalent Cassegrain, the very fast optical system leads to a tight collimation and focus error budget. The performance target is for 0.1-arcsecond rms images over the entire 15-arcminute field. This translates into a required positioning

accuracy of 2.5-$\mu m$ despace, 17-$\mu m$ decenter, and 10-arcseconds of tip. Although the on-axis zero-coma condition can be used to relax the decenter and tip constraints, it is not a good idea for a fast telescope with a wide field of view.[14-15] As a consequence, we chose the optical alignment procedure to independently null tip and decenter with respect to the optical axis of the primary mirror. The procedure was simple and utilized the fact that the Gregorian prime focus is between the primary and secondary mirrors. A snout was attached to the center hub of the secondary mirror that contained a CCD spaced from the vertex precisely at the prime focus position. The mirror and CCD were attached to a high precision rotary stage and the exact CCD pixel that went through the secondary optical axis was located. Then the CCD was positioned precisely at the prime focus point through direct imaging. Due to extremely large field-dependent coma at the f/1.0 prime focus, the center of the field was readily identified. The snout was removed and the positioner was programmed to rotate the secondary vertex about the prime focus until the field coma was removed at the f/9 focus. This quick and successful procedure insures that the primary and secondary optical axes are coincident.

## 8.0 Wavefront Sensing

Given the relatively small size and high stiffness of the VATT's optical support structure and primary mirror, a low-resolution wavefront sensor for nightly routine collimation should be unnecessary. Instead we built a high resolution wavefront sensor to be used for annual or semi-annual calibration of collimation look-up tables for the secondary positioner vs. elevation and diagnosis of imaging problems should they arise. The device is shown in Figure 10 and is based

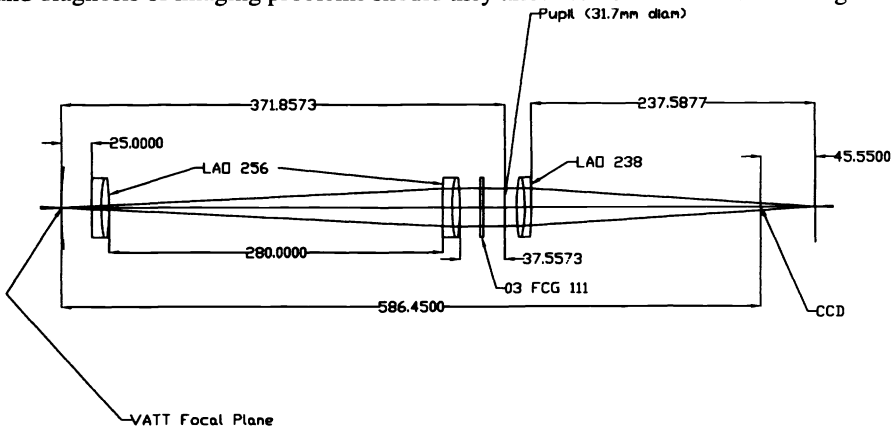


**FIGURE 10. The optics for the VATT interferometric Hartmann wavefront sensor consist of a simple Petzval collimator that produces a pupil where the Hartmann mask is located. A single doublet converges the light from the Hartmann apertures towards a common focus. A CCD camera is placed about 45.5-mm inside of this focus where the interferogram is produced. The bandpass of the device is defined by the blue cutoff of the filter (700-nm) and the red cutoff of the CCD. A two-position turret placed at the focal plane selects from a pinhole aperture or a laser diode source to create either a star or a reference interferogram respectively.**

on the interferometric Korhonen-Hartmann technique developed at the Nordic Optical Telescope (NOT).[16-18]

This type of wavefront sensor differs from the traditional Shack-Hartmann design in that it directly measures phase (rather than slopes). Light coming out of the Hartmann apertures is converged toward a common focus. Each adjacent quadruplet of apertures forms a 2-dimensional interference pattern that consists mainly of a small m=0 spot. Spacing irregularities between interference spots are used to calculate the phase difference between apertures. At a certain distance either inside or outside of this common focus, the m=0 interference fringe of one quadruplet of apertures overlaps the m=±1 fringe of the adjacent interference pattern. The detector is located in this plane. In order to minimize contamination from overlapping m=1 fringes on the m=0 fringe position, the aperture size and geometry is chosen so that the m=1 interference fringes are suppressed by the $\text{sinc}^2$ envelope of the aperture diffraction.

The NOT instrument incorporates a beam splitter at the telescope focus in order to feed a reference light source into the device. This introduces spherical aberration, and the transfer optics were designed to remove it. We chose instead to place a two-position turret at the telescope focus that selects from a diode laser source or a pinhole. The pinhole is

placed into the center of a 45-degree mirror so that an auxiliary camera may be used for direct viewing. As a consequence, the optical design is simpler and off the shelf lenses were used. The analysis software was purchased from Opteon, Inc. (Piikki, Finland).

Typical reference and stellar interferograms are shown in Figure 11 along with a geometric spot diagram obtained shortly after the secondary mirror was installed. Despite virtually no optimization of the telescope or environment, we

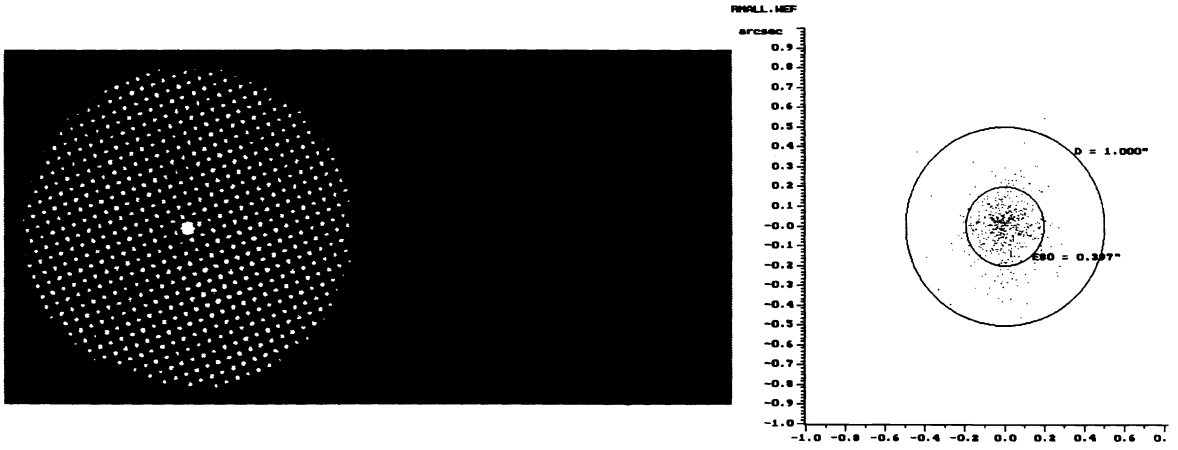


**FIGURE 11. Typical wavefront sensor interferograms produced by the laser diode (left) and a star (center--the vane shadow at 8:30 was the temporary secondary cabling bundle.). The geometric spot diagram shown (right) was produced shortly after the telescope became operational in late 1994. The atmosphere was removed by averaging 18 0.5-sec stellar interferograms and subtracting the laser reference. At that time the 80% encircled energy diameter was less than 0.4-arcseconds. No recent interferograms have been obtained despite several improvements in the telescope and environment.**

realized 0.4-arcsecond 80% encircled energy diameter images from the telescope optics once the atmosphere was removed. Due to other priorities, the wavefront sensor has not been used during the past year, so accurate collimation look-up tables have not yet been produced.

## 9.0 Imaging

Figure 12 shows a wide-field image taken with the VATT and field-flattened 2k x 2K CCD.

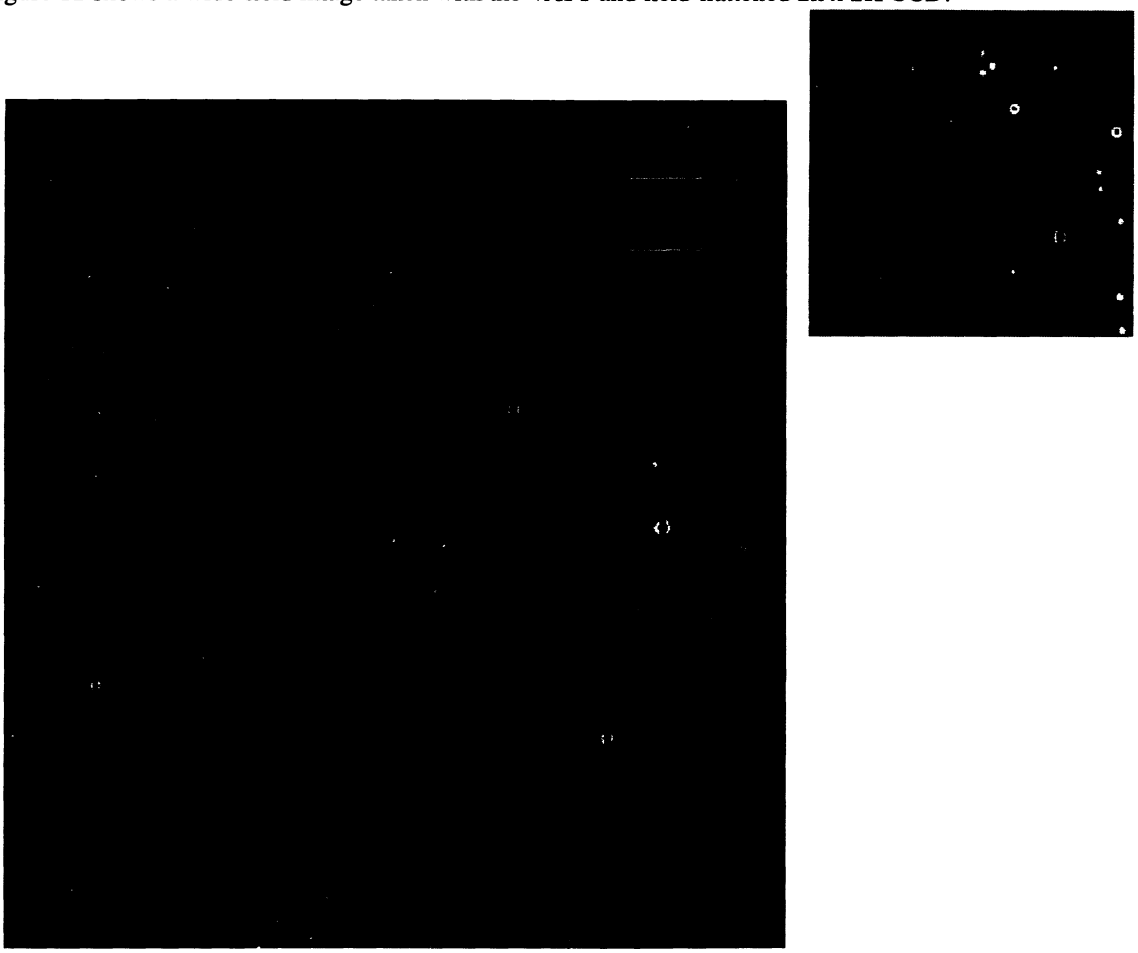

**FIGURE 12. 20 direct 11 x 11 arcminute R-band images stacked on top of each other in the bulge of M31 taken with the VATT and a 2K x 2K CCD equipped with a field-flattener (galaxy surface brightness removed). Each exposure was approximately 15-min long and manually guided. The resulting image retains 1.0-arcsecond FWHM PSF across the entire field. A 1 x 1 arcminute enlargement near the field corner illustrates wide-field telescope performance in tracking, de-rotating, and collimation. Photo: courtesy of Austin Tomaney.**

## 10.0 Acknowledgments

We acknowledge the excellent work of the Steward Observatory technical division, the Steward Observatory Mirror Laboratory, the Mount Graham International Observatory crew led by John Ratje, and the efforts of Buddy Powell, George Coyne, and Peter Strittmatter.

## 11.0 References

1. H. M. Martin, D. S. Anderson, J. R. P. Angel, R. H. Nagel, S. C. West, and R. S. Young 1990, "Progress in the Stressed Lap Polishing of a 1.8-m f/1 Mirror," Proc. SPIE, *Advanced Optical Technology Telescopes IV*, **1236**, 682.

2. H. M. Martin, D. S. Anderson, J. R. P. Angel, J. H. Burge, W. B. Davison, S. T. DeRigne, B. B. Hille, D. A. Ketelsen, W. C. Kittrell, R. McMillan, R. H. Nagel, T. J. Trebisky, S. C. West, and R. S. Young 1992, "Stressed Lap Polishing of a 1.8-m f/1 and 3.5-m f/1.5 Primary Mirrors," *ESO Conference on Progress in Telescope Instrumentation Technologies*, p 169, April 27-30, Garching Germany, ed. M. H. Ulrich.

3. S. C. West, J. H. Burge, R. S. Young, D. S. Anderson, C. Murgiuc, D. A. Ketelsen, and H. M. Martin 1992, "Optical Metrology of Two Large Highly Aspheric Telescope Mirrors," *Applied Optics* **31**, 7191.

4. S. C. West, H. M. Martin, R. H. Nagel, R. S. Young, W. B. Davison, T. J. Trebisky, S. T. DeRigne, and B. B. Hille 1994, "Practical Design and Performance of the Stressed-Lap Polishing Tool," *Applied Optics* **33**, 8094.

5. D. Vukobratovich, B. Iraninejad, R. M. Richard, Q. M. Hansen, and R. Melugin 1982, "Optimum shapes for lightweighted mirrors", Proc. S.P.I.E. **332**, *Advanced Technology Optical Telescope*s, 419-423.

6. D. Anderson, R. E. Parks, Q. M. Hansen, and R. Melugin 1982, "Gravity deflections of lightweighted mirrors", Proc. S.P.I.E. **332**, *Advanced Technology Optical Telescope*s, 424-435.

7. Space Optics Research Lab Certificate of Conformance. Model 0-31009, May 28, 1992.

8. "Columbus project finite element analysis of a 1.8-m f/1.0", BCV #1 (R0), 1986 Nov.; pg. 51 and figures 2-51 and 2-52.

9. G. Ballio and G. Parodi 1988, "Lateral Support Optimization of a 1.8-m f/1 Equatorial Mirror", BCV (the relevant models are found on page 10 and figures 19-23.

10. J. R. P. Angel, A. Y. S. Cheng, and N. J. Woolf 1988, "Thermal stabilization of honeycomb mirrors", in *Proc. ESO conference on very large telescopes and their instrumentation*, ed. M.H. Ulrich, 467.

11. M. Lloyd-Hart 1990, "System for precise temperature sensing and thermal control of borosilicate honeycomb mirrors during polishing and testing", *Advanced Technology Optical Telescopes IV*, Proc. S.P.I.E. **1236**, ed. L. D. Barr, 844.

12. J. M. Hill 1990, "Optical design, error budget and specifications for the Columbus project telescope", Proc. S.P.I.E. **1236**, *Advanced Technology Optical Telescopes IV*, 86.

13. D. Blanco, C. Corbally, R. Nagel, and W. Woolf 1990, "Advanced Technology in the VATT", Proc. S.P.I.E **1236**, *Advanced Technology Optical Telescopes IV*, 905-911.

14. R. Bhatia, May 1995, "Is the zero-coma condition sufficient?", Telescopio Nazionale Galileo Technical Report #43, Astronomical Observatory Pavoda-Asiago.

15. B. A. McLeod 1996, "Collimation of Fast Wide-Field Telescopes", *Publ. A.S.P.* **108**, 217-219.

16. T. K. Korhonen 1984, "Interferometric method for optical testing and wavefront error sensing", Proc. S.P.I.E. 444, *Advanced Technology Optical Telescopes II*, 249-252.

17. T. K. Korhonen, S. T. Haarala, J. O. Piironen, and A. K. Sillanpaa 1986, "Proc. S. P. I. E. **628**, *Advanced Technology Optical Telescopes III*, 486-491.

18. T. K. Korhonen, T. Lappalainen, and A. Sillanpaa 1991, "Hartmann interferometric testing of large mirrors", Proc. S.P.I.E. **1531**, *Advanced Optical Manufacturing and Testing II*, 44-49.